IEEE Access
Multidisciplinary | Rapid Review | Open Access Journal

Received 18 July 2022, accepted 3 August 2022, date of publication 9 August 2022, date of current version 16 August 2022.

Digital Object Identifier 10.1109/ACCESS.2022.3197630

RESEARCH ARTICLE

Magnetic Anomaly Detection Method Based on Feature Fusion and Isolation Forest Algorithm

NING ZHANG[1], YIFEI LIU[1], LEI XU[2], PENGFEI LIN[3], HEDA ZHAO[4], AND MING CHANG[1]

[1]College of Weapons Engineering, Naval University of Engineering, Wuhan 430033, China
[2]Unit 92859 of PLA, Tianjin 300061, China
[3]Department of Hydropower and Chemical Defense, Dalian Naval Academy, Dalian 116000, China
[4]Unit 91977 of PLA, Beijing 100000, China

Corresponding author: Yifei Liu (lyf1016505829@163.com)

This work was supported in part by the National Natural Science Foundation of China under Grant 6217011665.

ABSTRACT In order to improve the weak magnetic detection ability under the background of Gaussian colored magnetic environment noise, a magnetic anomaly detection method based on feature fusion and isolation forest (IForest) algorithm is proposed in this paper. The method uses different feature algorithms to extract the statistical features, time-frequency features and fractal features of the signal, reduces the dimensionality of the features by principal component analysis (PCA) and generates feature fusion tensors. Finally the IForest algorithm is used to achieve target detection. The simulation and experimental results show that the method has a higher detection rate under different SNR of Gaussian color noise, which is approximately 5%-18% higher than that of the traditional feature detection algorithm. This method can train an effective detection model with only a small number of negative samples. Compared with the fully connected neural network (FCN) model trained with unbalanced samples, the detection rate increases by approximately 5%-12%, and it takes less time.

INDEX TERMS Magnetic anomaly detection, feature fusion, unsupervised learning, isolation forest, principal component analysis.

I. INTRODUCTION

Magnetic anomaly detection is widely used in geological exploration, anti-submarine investigation and other fields due to its high concealment, strong anti-natural interference ability, and good regionality [1]. Aeromagnetic anomaly detection is one of the main forms of magnetic anomaly detection [2], but due to the long detection distance, the target signal is very weak compared to the background magnetic field. The influence of factors such as the background noise of the magnetic detector and the changing field of the geomagnetic field increases the difficulty of target detection.

Experts have done a lot of research on improving the weak magnetic detection ability. Ginzbug first proposed that a set of standard orthonormal basis functions (OBF) can be used to accurately describe the magnetic dipole signal [3], and the energy detector was constructed by using the squared sum of the decomposition coefficients of the OBF. However, this algorithm can only achieve better results in the background of Gaussian white noise. The actual magnetic noise is mostly colored noise with a power spectral density of $1/f^{\alpha}$ [4]. So [5] proposed to use the Kahennan-Lovey expansion to correct the standard orthonormal basis function according to the autocorrelation coefficient of the geomagnetic noise, which adapting OBF detectors to colored noise better. However, in the actual detection process, the shortest distance and relative motion state between the non-cooperative target and the platform are difficult to estimate, which leads to the limitation of this method. Tang Y, Pan M C, etc. have studied detection algorithms based on magnetic background noise, such as minimum entropy filtering [6], [7], stochastic resonance [8], etc., which using the statistical characteristics of magnetic background noise, but its performance is easily limited by low SNR [9]. Most of these traditional detection methods are based on the detection of a single feature, which cannot make full use of the information in the signal, and are often only suitable for specific environmental noise.

The associate editor coordinating the review of this manuscript and approving it for publication was Yongming Li.

In recent years, many scholars have studied the method of using machine learning to extract multi-domain features of target signals to achieve target detection [10]. Reference [11] converts the original signal into a two-dimensional image through Wigner-Ville time-frequency transformation, and uses CNN to achieve classification detection. Although the detection performance is improved, the image processing will occupy a lot of computing resources, and the efficiency is low, which cannot meet the needs of real-time detection. The article [12] designed a CNN with residual structure, which can directly process one-dimensional signals and shorten the calculation time. Reference [13] uses FCN to automatically extract the multi-domain features of the target signal, which improves the detection rate under the colored noise background. These methods can establish a more complex nonlinear relationship between the multi-domain features of the signal, so as to better ensure the detection effect under different noises. However, most of these methods have high requirements on the quality and quantity of samples, and the effect is poor under the condition of uneven positive and negative samples in the training set, so the practicability is not strong.

In this paper, a magnetic anomaly detection method based on feature fusion and IForest algorithm is proposed. Firstly, the real-time signal is intercepted into several time series samples through a sliding window, and the time-frequency features, statistical features, fractal features of each sample is extracted. Then use PCA to reduce the feature dimension, and finally input it into the pre-trained IForest detector to complete the target detection. Based on the simulation data set, the influence of feature dimension, the number of isolation trees (iTrees), and the maximum number of samples on IForest is studied to optimize the parameter settings. Through simulation and design experiments, the performance of this method is compared with several existing detection methods. The feasibility and superiority of the method are verified.

II. AEROMAGNETIC ANOMALY DETECTION MODEL

During aeronautical magnetic detection, as the relative position of the target and the magnetic detector changes, the magnetic signal changes regularly, and the target is detected by processing and analyzing the measured signal. The process is modeled as shown in Fig.1.

Under normal circumstances, the effective detection distance of an aviation magnetometer is more than 600m, far exceeding the size of the target. According to the paper [14], the target can be equivalent to a magnetic dipole. Under this condition, a Cartesian coordinate system is established with the target position as the origin, and the magnetic induction intensity $\vec{B}$ generated at the spatial point (x, y, z) is:

$$\begin{cases} B_x = \dfrac{100}{r^5}\left[(3x^2 - r^2)M_x + 3xyM_y + 3xzM_z\right] \\ B_y = \dfrac{100}{r^5}\left[3xyM_x + (3y^2 - r^2)M_y + 3yzM_z\right] \\ B_z = \dfrac{100}{r^5}\left[3xzM_x + 3yzM_y + (3z^2 - r^2)M_z\right] \end{cases} \quad (1)$$

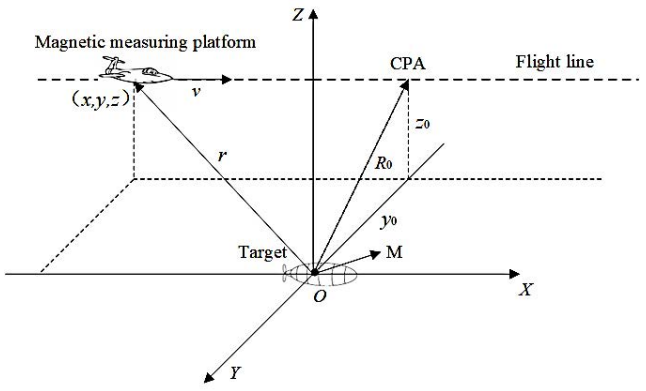

FIGURE 1. Aeromagnetic anomaly detection model.

where distance $r = \sqrt{x^2 + y^2 + z^2}$, magnetic moment $M = (M_x, M_y, M_z)^\top$.

Without considering the background magnetic interference and the background noise of the magnetic detector, the output value of the optical pump magnetic detector carried on the aviation platform is the modulus value of the combined magnetic field $\vec{T}$ of the target magnetic anomaly $\vec{T_a}$ and the geomagnetic field $\vec{T_0}$, which is:

$$\Delta T = \left|\vec{T}\right| - \left|\vec{T_0}\right| \quad (2)$$

Simplified from the cosine theorem, we get:

$$\Delta T = \left|\vec{T_a}\right| \cos\theta \quad (3)$$

That is, the measured magnetic anomaly ΔT is the projection of $\vec{T_a}$ on the direction of the geomagnetic field. By consulting the data, it can be seen that the direction change of the magnetic field $\vec{T_0}$ in the area of 10000 km^2 is less than 1°, so the direction angle θ of the geomagnetic field can be regarded as a fixed value [15]. Denote θ by the magnetic inclination angle I and the magnetic declination angle D, according to the spatial triangular relationship ΔT can be expressed as:

$$\Delta T = B_x \cos I \cos D + B_y \cos I \sin D + B_z \sin I \quad (4)$$

It shows that the amplitude of the magnetic anomaly signal is affected by the target magnetic moment, magnetic inclination, magnetic declination and other factors, and changes with the relative position of the target and the magnetic detector.

However, the signal is often polluted by colored noise. This is because the interference of the sensors' background noise and the short-term change of the geomagnetic field [16] makes the power spectrum of the actual noise not evenly distributed in each frequency band but is decremented by $1/f^\alpha$ $(0 < \alpha < 2)$ [17]. In this case, traditional detection methods do not work well [5].

The use of machine learning method for magnetic anomaly detection can solve this problem. As long as the sample coverage is wide enough, the method can better adapt to various environmental noises. Correspondingly, the effect of this

method is greatly affected by the number and quality of samples [18]. In practical applications, the label information of most of the obtained samples is unknown, so it is difficult to use supervised learning methods to train the model. In addition, due to the high cost of acquiring positive samples (mixed signals containing targets), the sample size is small while the number of negative samples (pure background noise) is large, the detection performance of the model trained with imbalanced samples will be greatly reduced. Therefore, this paper proposes a real-time magnetic anomaly detection method based on feature fusion and IForest algorithm, which fully mines the sample information through unsupervised learning, and has important theoretical value and application prospects.

III. MAGNETIC ANOMALY DETECTION METHOD BASED ON FEATURE FUSION AND IFOREST ALGORITHM

A. FEATURE FUSION

Feature fusion is to use different feature extraction algorithms to obtain different features of magnetic anomaly signal, then fuse these features to reduce the dimension, and use the fused feature values as the input of the target detection model [19].

1) FEATURE EXTRACTION

Feature extraction can suppress noise interference and reduce information redundancy. The selected features need: strong interpretability of the original signal, high degree of division, insensitivity to noise changes. Accordingly, this paper selects the statistical features [16], time-frequency features [20], and fractal features [21] as the basis for target detection.

Zero-crossing analysis is an analysis method based on the statistical characteristics of the signal. The zero-crossing rate refers to the number of times that the signal passes through the zero value after removing the linear component per unit time [22]. Suppose a time series $x(n)$, $n = 1, 2, \ldots N$, and the operator $\chi[\cdot]$ is defined such that:

$$q(n) = \chi[x(n)] = \begin{cases} 1, & x(n) > 0 \\ 0, & x(n) \le 0 \end{cases} \tag{5}$$

Then the number of zero crossings of the signal $x(n)$ is:

$$D = \sum_{n=2}^{N} [q(n) - q(n-1)]^2 \tag{6}$$

Obviously, $0 \le D \le N-1$, The zero-crossing rate is defined as:

$$R = \frac{D}{N-1} \tag{7}$$

Define the k-order difference operator ∇^k, The zero-crossings are extended to higher orders by the following recursion:

$$\begin{cases} \nabla x(n) = x(n) - x(n-1) \\ \nabla^k x(n) = \nabla[\nabla^{k-1} x(n)], \quad k = 2, 3, \ldots, K \end{cases} \tag{8}$$

Among them, K is the maximum difference order. The length of $\nabla x(n)$ is $N-1$ while the length of $\nabla^k x(n)$ is N-k. Defining the zero-crossing number of differential time series $\nabla^{k-1} x(n)$ is D_k, then its zero-crossing rate is:

$$R_k = \frac{D_k}{(N-k)} \tag{9}$$

The time-frequency feature provides information on the signal variation with time of different frequency components. The commonly used analysis methods include short-time Fourier transform, wavelet packet analysis, etc [23]. Consider its advantages in handling non-stationary time-varying signals [24], the paper uses wavelet packet analysis to extract the time-frequency characteristics of the signal. The principle of the algorithm is to use a set of wavelet coefficients to approximate the signal to be analyzed:

$$\psi_{a,b}(t) = \frac{1}{\sqrt{|a|}} \psi\left(\frac{t-b}{a}\right), \quad a, b \in R, a \ne 0 \tag{10}$$

Among them, $\psi(t)$ is the base wavelet function. Parameter a is the scale parameter, which reflects the period length of the wavelet and corresponds to the frequency domain information of the signal; b is the translation parameter, which controls the appearance position of the wavelet in the time domain by shifting, reflecting the time domain information. The wavelet packet decomposition process is realized by recursion, which is equivalent to convolving the wavelet packet coefficients with the paired high-pass filter $G(k)$ and low-pass filter $H(k)$. The formula is as follows:

$$\begin{cases} w_{j,2m}(n) = \sqrt{2} \sum_{k \in Z} H(k-2n) w_{j-1,m}(k) \\ w_{j,2m+1}(n) = \sqrt{2} \sum_{k \in Z} G(k-2n) w_{j-1,m}(k) \end{cases} \tag{11}$$

Among them, $w_{j,m}(n)$ represents the wavelet packet coefficient of the mth node of the jth decomposition layer. And the larger the amplitude is, the more similar the signal at the corresponding frequency band and time domain position is to the wavelet packet function. According to the literature [15], the sym6 wavelet base is suitable for multi-scale decomposition of aeromagnetic signals, so this paper selects the sym6 wavelet base, and the number of decomposition layers is 4.

The essence of fractal characteristics is the self-similarity of the research object, which is a supplement to the statistical characteristics and time-frequency characteristics of signals [25]. Geomagnetic noise has obvious long-range autocorrelation between local and local [21]. Noise and mixed target signals can be distinguished by extracting fractal features. In this paper, the fractal features of the signal are extracted by calculating the box dimension. The calculation method of the box dimension of the time series is as follows:

(1) Suppose a time series $x(n)$ of length N is measured. Normalize its amplitude and time scale and then put it into a square.

(2) Select a grid consisting of boxes with side length ε_m, $m = 1, 2, \ldots, M$, cover the unit square in (1) with the grid, and record the number of intersections of each size box with $x(n)$, denoted as $N_m(\varepsilon_m)$.

(3) Calculate $D_B = \ln N_m(\varepsilon_m) / (-\ln \varepsilon_m)$, if $x(n)$ is a regular fractal, the relationship between $\ln N_m(\varepsilon_m)$ and $\ln \varepsilon_m$ on the double logarithmic coordinate system is a straight line, and D_B is the slope of the straight line.

2) PCA FUSION DIMENSIONALITY REDUCTION

There are usually strong correlation features in the extracted signal features, which will interfere with the detection effect and increase the amount of calculation. Therefore, we use the PCA algorithm to compress the extracted feature values to simplify the model input.

The core idea of PCA is to find a set of k-dimensional new basis ($k < n$) which any two basis vectors satisfy linear independence in the original n-dimensional space., so that the original feature is mapped to this set of bases with the largest variance, and the projection of the original data on the new base is the dimension-reduced data. Suppose there are mn-dimensional vectors x_i ($1 \le i \le m$) in a dataset X:

$$X = \begin{bmatrix} x_1^\top \\ \vdots \\ x_m^\top \end{bmatrix}, x_i \in R^n \tag{12}$$

The dimensionality reduction process can be expressed as:

$$y_i = W x_i \tag{13}$$

where $y_i \in R^k$ and $k < n$, then

$$W = \begin{bmatrix} w_1^\top \\ \vdots \\ w_k^\top \end{bmatrix} \in R^{k \times n} \tag{14}$$

The derivation shows that in order to maximize the variance after mapping the original data to w, the eigenvectors corresponding to the largest k eigenvalues should be selected to form W [26], and then the dimensionality-reduced data can be obtained by formula(13). It can be seen that the principal components generated by PCA are linear combinations of the original features rather than a single feature. The principal components with a cumulative contribution rate greater than 95% after dimensionality reduction [27] are selected to form a feature fusion tensor.

B. FOREST MAGNETIC ANOMALY DETECTION ALGORITHM

IForest is an unsupervised learning algorithm based on decision trees that identifies anomalies by isolating outliers in data [28]. In the process of magnetic detection, due to the short duration of the magnetic anomaly target signal, the data distribution is sparse and far from pure noise data clusters with high density, such samples will be isolated after a few random feature divisions, resulting in shorter paths in the tree. Therefore, by calculating the average path length, the normal value and the abnormal value can be distinguished, and the target detection can be realized. The algorithm principle is shown in Fig.2.

The algorithm is divided into two phases, training and anomaly detection [29]. Training is to use the training set

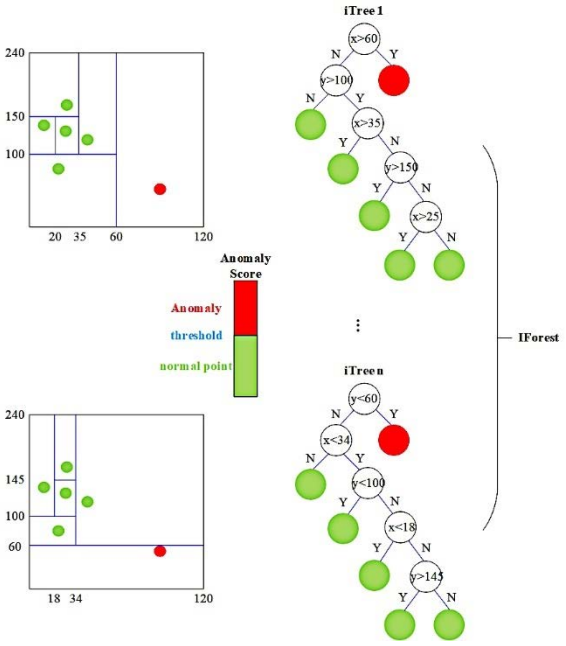

FIGURE 2. IForest detection principle.

data to generate several iTrees to form IForest, each iTree is a binary tree structure, representing several division methods of sample points. During anomaly detection, the test set samples are brought into each iTree, the average path length and anomaly score are calculated, and the threshold is used to determine whether it is anomaly. The specific process is as follows:

(1) Randomly select n samples from the training sample set and put them into the root node of an iTree. Set the maximum value in the sample data to be $x_{\max}$ and the minimum value to be $x_{\min}$.
(2) Randomly select one dimension of the sample data and a certain dividing point $P(x_{\min} < P < x_{\max})$ under this dimension, and divide the node data into two subspaces: put the samples with data less than P into the left node while put the sample greater than or equal to P into the right node.
(3) Repeat (1)-(2) recursively in the child nodes, and continuously generate new child nodes until there is only one sample in each node or the limit tree height is reached.
(4) Cycle (1)-(3) to continue training the next iTree until the specified number of iTrees are generated.
(5) The average height c(n) of each iTree is calculated to normalize the average path length of all sample points, as shown in equation (15).

$$c(n) = \begin{cases} 2\left[H(n-1) - (n-1)/n\right], & n > 2 \\ 1, & n = 2 \\ 0, & otherwise \end{cases} \tag{15}$$

where $H(i)$ is the harmonic number, which can be estimated by $H(i) = \ln(i) + \zeta$, Euler–Mascheroni constant $\zeta \approx 0.577$.

(6) Input the sample to be detected into the trained IForest model, make it traverse each iTree, calculate the path length $h(x)$ of the sample x, and obtain the abnormal score $s(x, n)$ of the sample, the formula is as follows:

$$s(x, n) = 2^{-\frac{E(h(x))}{c(n)}} \tag{16}$$

$E(h(x))$ is the expectation of the path length $h(x)$. $h(x)$ is equivalent to the number of divisions required to isolate a sample point. The closer $s(x, n)$ is to 1, the greater possibility that the sample point is abnormal.

C. PRINCIPLE OF MAGNETIC ANOMALY DETECTION METHOD BASED ON FEATURE FUSION AND IFOREST

Since the smallest unit processed by the method in this paper is the sample, consider using a sliding window to subdivide the data into multiple time series samples so that realize real-time detection. The sliding window should contain the complete target signal without introducing too much noise. So its size should be set according to the duration of the target signal which is calculated according to $3 \times \mathrm{CPA}/v$ [30]. The selected window length is usually slightly larger than the effective duration, and the difference between the two is the window moving step, ensuring that there is always a window that can contain the complete target signal.

Fig.3 shows the flow of the detection method proposed in this paper. Firstly, the geomagnetic noise lasting a period of time is divided into several samples of the same length through a sliding window. Then extract the statistical features, time-frequency features and fractal features of the sample signal and use PCA to fuse the extracted features to construct a feature fusion tensor. Set the model parameters (number of iTrees, maximum number of samples, etc.) to train the iForest model. In the detection process, the input signal also need to be processed by segmentation, feature extraction, and PCA. Then the trained iForest model is used to complete the target detection according to the threshold determined by the N-P criterion.

IV. SIMULATION AND EXPERIMENTAL VERIFICATION

A. SIMULATION

1) SIMULATION DESIGN

The sampling rate of the optical pump magnetic detector is generally 20Hz, the cruising speed of the platform is about 320-380km/h, and the effective range of the magnetic detector can reach 600m-900m [31]. According to this, the simulation parameters of the underwater magnetic anomaly target are set, such as TABLE 1 shown.

For the non-cooperative target, the information such as relative position, and the angle between magnetic moment direction and the detection path is unknown. In order to be close to the real situation and test the generalization performance of the method, the samples should cover as many situations as possible. Set Gaussian color noise conditions, repeat the simulation 6000 times under different magnetic moment directions for the target signal superimposed with the set noise, that is, generate 6000 positive samples under each noise condition. The simulation is repeated 11,000 times for the pure Gaussian color noise to generate 11,000 negative samples. Change the noise conditions and simulate in the same way to generate sample sets under different noise conditions. The training set and test set required for the different methods used in the following sections are divided as shown in TABLE 2, in which local outlier factor (LOF) and high-order zero-crossing detection (HOC) do not require training.

TABLE 1. Simulation parameter settings.

Target simulation conditions	Numerical value
Target magnetic moment (A·m^2)	(6.2, -0.1, 1.5) ×10^5
Geomagnetic dip (°)	45
Magnetic declination (°)	0
Lateral distance (m)	0
Vertical distance (m)	600
Cruise speed (m/s)	100
Sampling rate (Hz)	20

TABLE 2. Sample set division.

Algorithm	Training set (Number of positive samples/Number of negative samples)	Test set (Number of positive samples/Number of negative samples)
PCA-IForest	0/10000	1000/1000
FCN (1:1)	5000/5000	1000/1000
FCN (1:19)	500/9500	1000/1000
LOF	/	1000/1000
OS	0/10000	1000/1000
HOC	/	1000/1000

When extracting features, try to choose the value that makes the difference between the noise and the mixed signal as large as possible. The high-order zero-crossing rate, wavelet packet coefficient and box dimension of pure noise signal and mixed signal are calculated under the Gaussian color noise with SNR of 0dB and noise index α of 0.9, as shown in Fig.4. According to Fig.4, the first 10-order zero-crossing rate is selected as the statistical eigenvalue. The wavelet packet coefficient of the first node (0-0.625Hz) of the fourth decomposition layer is selected as the time-frequency eigenvalue. Box dimensions which the side lengths of the square box are 2, 4, 8, 16, and 32 is selected as fractal eigenvalues.

The extracted features are fused and reduced by PCA. Because the units of different eigenvalues are different and the amplitudes are quite different, the data should be standardized before PCA [32]. The formula is:

$$x' = \frac{x - \overline{x}}{\sigma} \tag{17}$$

where $\overline{x}$ is the sample mean and σ is the variance of the data. The principal components with a cumulative contribution rate greater than 95% are used as the input of the IForest model. The IForest model is trained with the training set and then tested on the test set.

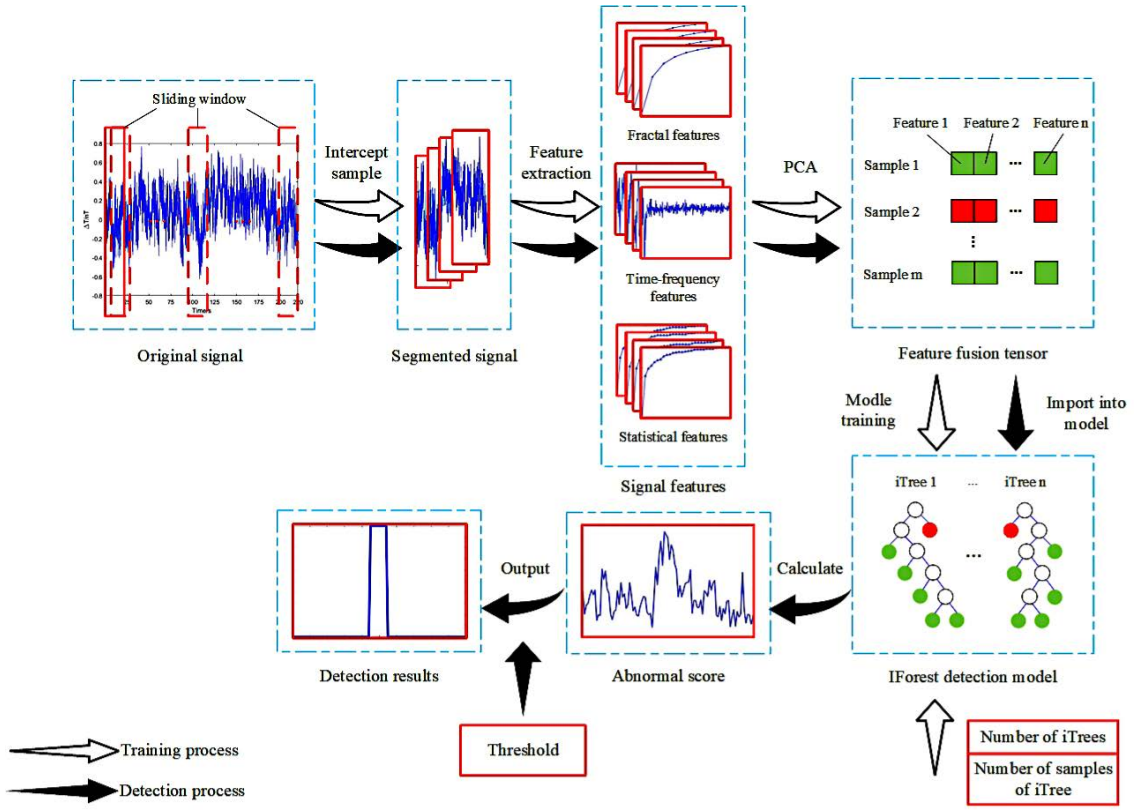

FIGURE 3. Method procedure.

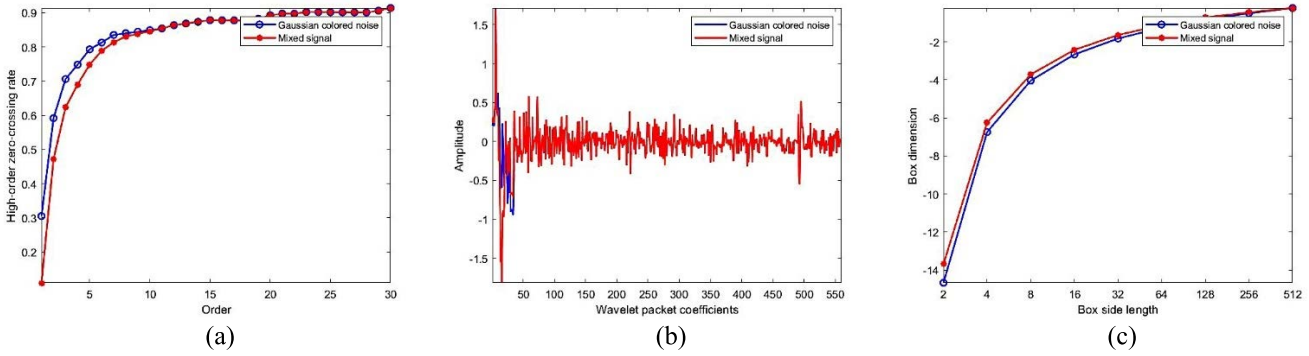

FIGURE 4. Feature extraction. (a) Zero-crossing rates, (b) Wavelet packet coefficients, (c) Box dimension.

2) PARAMETER OPTIMIZATION

This section studies the influence and optimization of the feature dimension, the number of iTrees and the maximum number of samples on the performance of the IForest algorithm. Let the number of positive samples in the detection samples be T and the number of negative samples be F; the number of samples determined by the algorithm as positive samples and the correct ones is TT; the number of samples determined by the algorithm as positive samples and the wrong ones is TF. The concepts of detection rate (TP), false alarm rate (FP), ROC curve, and AUC are:

$$TP = \frac{T}{TT} \tag{18}$$

$$FP = \frac{TF}{F} \tag{19}$$

The ROC curve is a curve composed of FP as the horizontal axis and TP as the vertical axis; AUC is the area under the ROC curve. The closer the AUC is to 1, the better the algorithm performance [33]. AUC is more stable than TP, so AUC is selected as the evaluation index when designing parameters. In addition, due to the high real-time requirements for the algorithm of the aeromagnetic detection, the calculation efficiency should also be considered in the parameter design.

The random selection of dimensions ensures that IForest can fully mine different feature information. But this

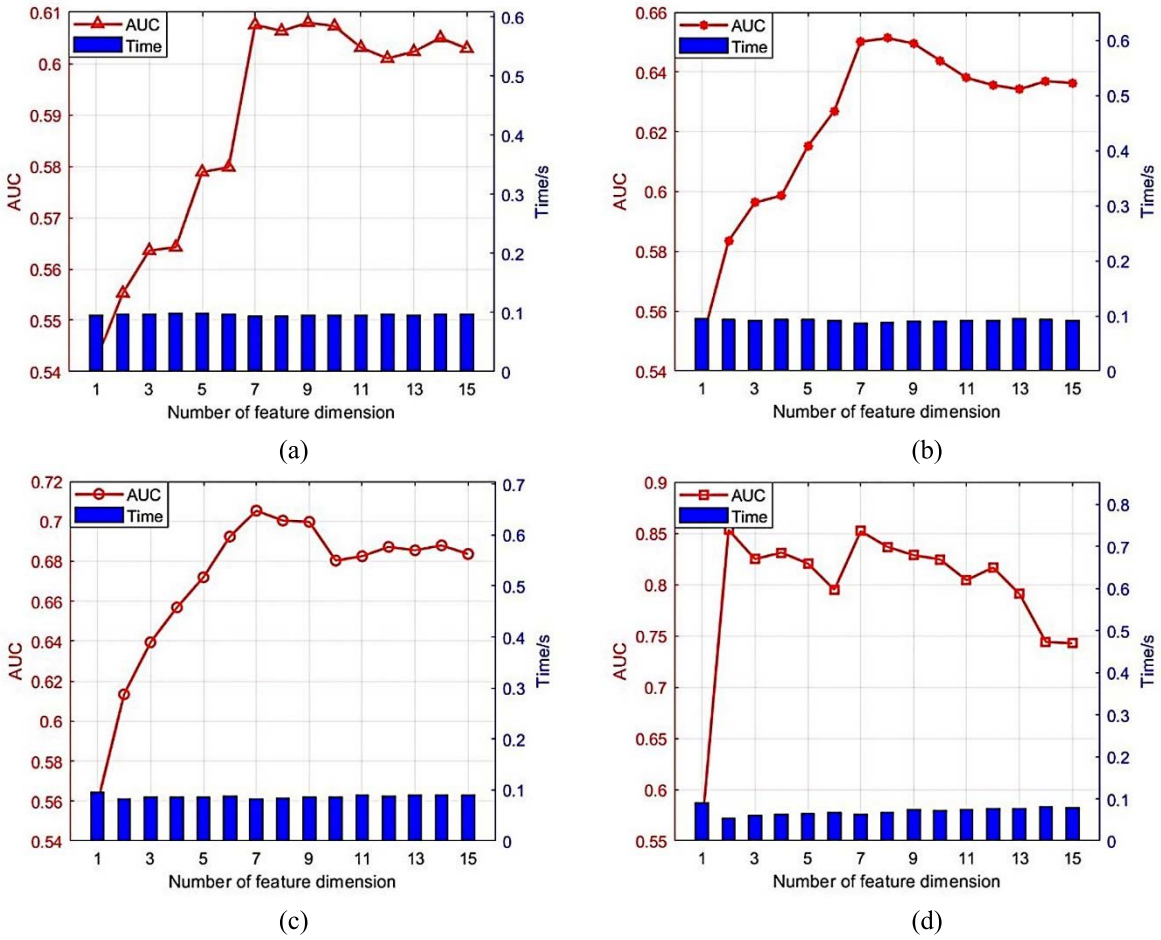

FIGURE 5. Selection of feature dimension. (a) The relationship between the number of feature dimension, AUC, and detection time($\alpha = 0.9$, SNR $= -10$dB), (b) The relationship between the number of feature dimension, AUC, and detection time($\alpha = 0.7$, SNR $= -10$dB), (c) The relationship between the number of feature dimension, AUC, and detection time($\alpha = 0.9$, SNR $= -5$dB), (d) The relationship between the number of feature dimension, AUC, and detection time($\alpha = 0.9$, SNR $= 0$dB).

randomness also introduces noise, which makes abnormal samples form denser clusters and confuse them with normal samples. Four different noise conditions are set, and the training and testing of the IForest model is completed according to the TABLE 2 sample division under each noise. The relationship between the number of feature dimension, AUC, and detection time is shown in Fig.5.

It can be seen that the AUC increases with the increase of the number of dimension and gradually becomes stable, and then the AUC decreases slightly. The higher the SNR and the smaller the color noise coefficient α, the earlier convergence occurs, indicating that when the noise interference is small, the ideal detection effect can be obtained by using fewer features, which is consistent with the actual situation. The detection time used for different number of dimensions is close. When the noise interference is small, the detection time is shortened, because the number of negative sample data segmentation is relatively small. In summary, the performance is the best when the first 7 principal components generated by PCA are selected as the input of the IForest model.

The number of iTrees determines the scale of the model, the larger the number, the more stable algorithm is. However, the number of iTrees is not as big as possible. Since each iTree has different ability to distinguish outliers, we only need to focus on iTrees that can distinguish positive and negative samples to a greater extent. Too many iTrees will waste computing power and reduce efficiency. The relationship between the number of iTrees and AUC and average abnormal score under the four noise conditions is as shown in Fig.6.

Fig.6 shows that when the number of iTrees is small, the model detection effect is poor, and the AUC fluctuate greatly. When the number of iTrees increases, AUC and the average abnormal score gradually converge, indicating that the model tends to be stable. As the number of iTrees increases, the detection time will increase proportionally, so the minimum value that makes the algorithm stable is selected, which is set to 100 in this paper.

The maximum number of samples is the number of samples used to train each iTree. As shown in Fig.7, the influence of this parameter on the detection performance under

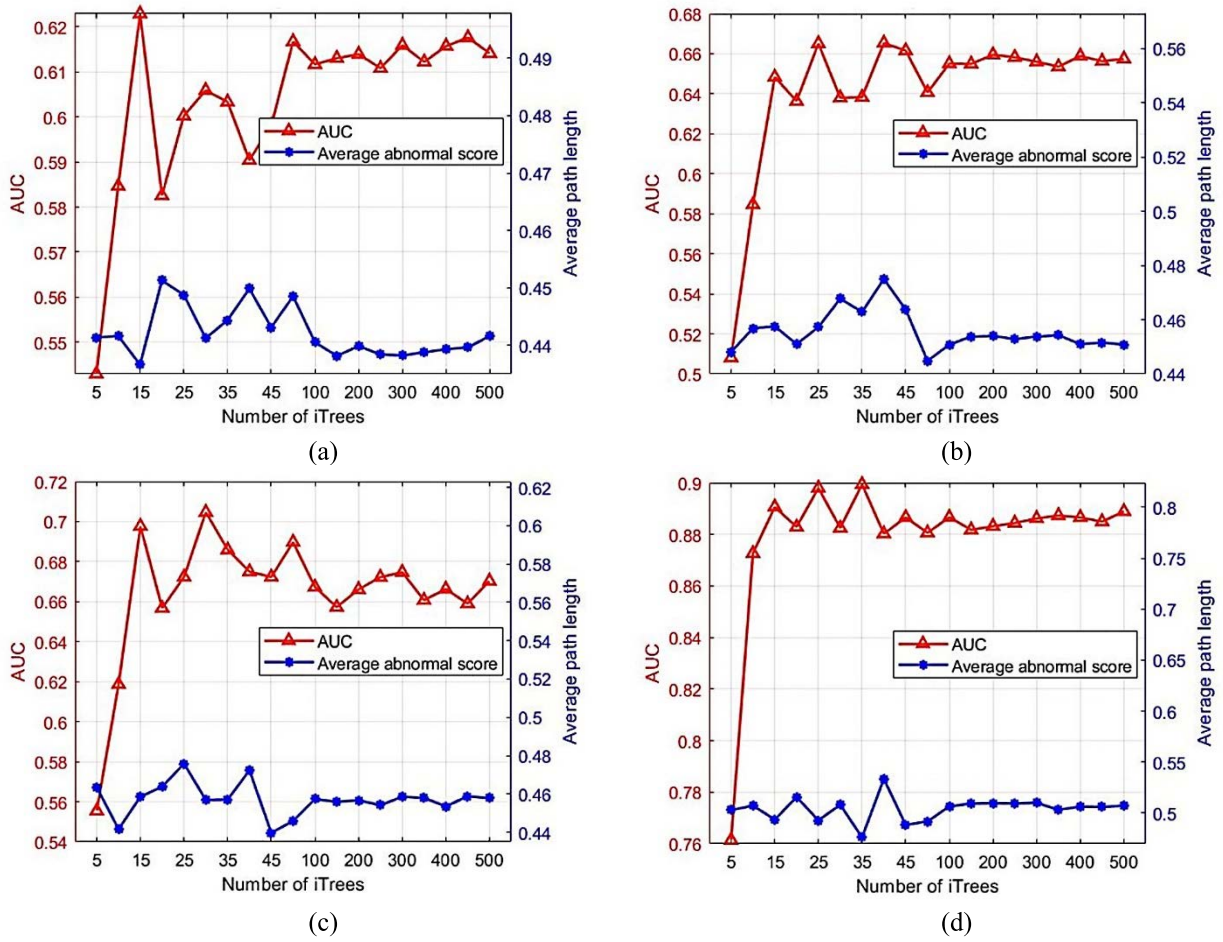

FIGURE 6. Selection of the number of iTrees. (a) The relationship between the number of iTrees, AUC, and path lengh($\alpha = 0.9$, SNR $= -10$dB), (b) The relationship between the number of iTrees, AUC, and path lengh ($\alpha = 0.7$, SNR $= -10$dB), (c) The relationship between the number of iTrees, AUC, and path lengh ($\alpha = 0.9$, SNR $= -5$dB), (d) The relationship between the number of iTrees, AUC, and path lengh ($\alpha = 0.9$, SNR $= 0$dB).

four noise conditions is studied. It can be clearly seen that AUC increases with the increase of the maximum number of samples and gradually converges. This is because more data segmentation methods are generated to mine more detailed information, but when the number is too large, a large number of similar iTrees will be generated, resulting in overfitting. In addition, when the maximum number of samples increases, the average path length of iTree increases and the detection time increases. According to this, the maximum number of samples is set to 512 in this paper.

3) SIMULATION RESULTS AND ANALYSIS

In order to verify the detection performance of the method in this article, compare it with other methods under different noise conditions. Firstly, two common unsupervised learning algorithms, LOF and One-class support vector machine (OS), are introduced to compare with the IForest algorithm. Fig.8 shows the ROC curves of the three algorithms and their respective AUCs. It can be seen that the AUC of the IForest algorithm is 2%-11% higher than that of the other two algorithms. When the noise interference is small, the advantage of IForest becomes weak, because the isolated data is random and the number of recursion is difficult to control. However, from the practical application point of view, the IForest algorithm is more suitable for the detection of magnetic anomalies in the background of low SNR color noise.

The detection method proposed in this paper is compared with the FCN in [13] and the HOC algorithm in [16]. We set different proportions of positive and negative samples in the FCN training set data to analyze its performance when the sample proportions are not balanced. Set $FP = 0.015$, and calculate the detection rates of three methods in different SNRs (color noise coefficient $\alpha = 0.9$) according to the N-P criterion, as shown in Fig.9 (a). It can be seen that when the ratio of positive and negative samples in training set is 1:1, the detection rate of FCN is much higher than the other two methods, but when the ratio is adjusted to 1:19, its detection rate drops significantly. This is because the FCN model will tend to reduce the loss of a large number of negative samples during iterative update in order to achieve the minimum loss

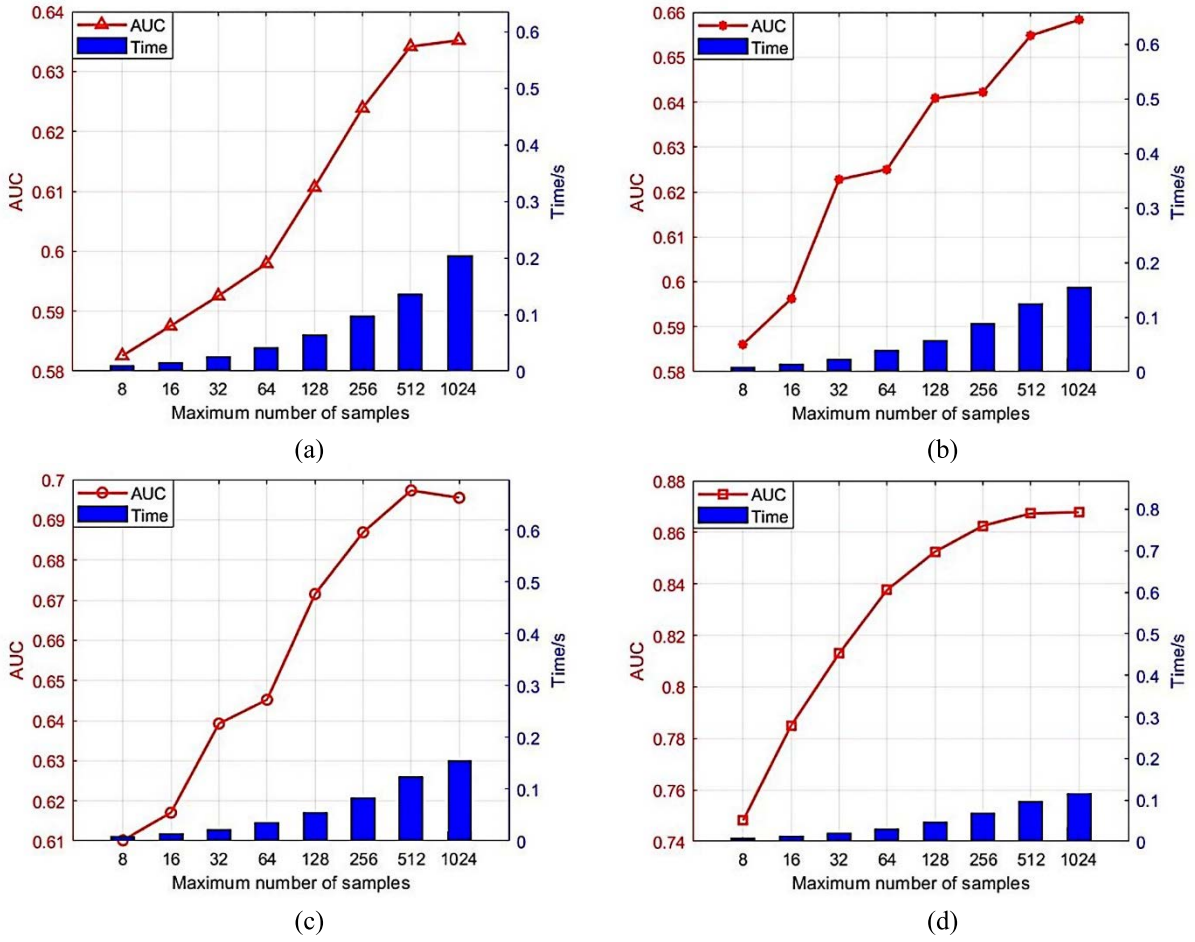

FIGURE 7. Selection of the maximum number of samples. (a) The relationship between the maximum number of samples, AUC, and detection time ($\alpha = 0.9$, SNR $= -10$dB), (b) The relationship between the maximum number of samples, AUC, and detection time ($\alpha = 0.7$, SNR $= -10$dB), (c) The relationship between the maximum number of samples, AUC, and detection time ($\alpha = 0.9$, SNR $= -5$dB), (d) The relationship between the maximum number of samples, AUC, and detection time ($\alpha = 0.9$, SNR $= 0$dB).

of full training samples, resulting in a decrease in the detection ability of positive samples. However, the ratio of positive and negative samples in the actually obtained magnetic data is much less than 1:19. So the advantages of method in this paper are highlighted. It only uses negative samples for training without affecting the ability to characterize sparse positive samples. Compared with FCN (1:19), the detection rate can be improved by 5%-12%, and this improvement is more obvious at low SNR. The detection rate of HOC is the lowest. Compared with HOC, the detection rate of the method in this paper increases by about 3%-20%, indicating that the fusion feature is more suitable for the detection of magnetic anomaly in the background of color noise.

Fig.9 (b) shows the total time of whole process of FCN and method in this paper under the same hardware environment. It can be seen that the time of this method is about 25%-35% of FCN, which is due to the fact that it does not involve complex iterative calculations, and with good linear time complexity. In addition, with the improvement of the SNR, the time-consuming of the method in this paper is gradually shortened while the FCN remains basically unchanged, indicating that the method in this paper is more flexible and more practical.

B. EXPERIMENT

1) EXPERIMENTAL DESIGN

The equipment used in the experiment mainly includes magnetic source, magnetic sensor, A/D conversion module, PC and so on. Limited by the existing conditions, a three-axis fluxgate sensor developed by the research group is used to replace the optical pump magnetometer. The sensitivity is 10pT/$\sqrt{}$Hz@1Hz, the resolution is 0.25nT, the dynamic range is $\pm$75000nT, and the sampling frequency is 400Hz. Its measurement error has been corrected. The magnetic source is an axially magnetized magnet with a magnetic moment of about 0.036A$\cdot$m^2. Data acquisition and processing are completed by the PC.

The experimental site is in a degaussing laboratory, where the magnetic environment is relatively uniform and stable.

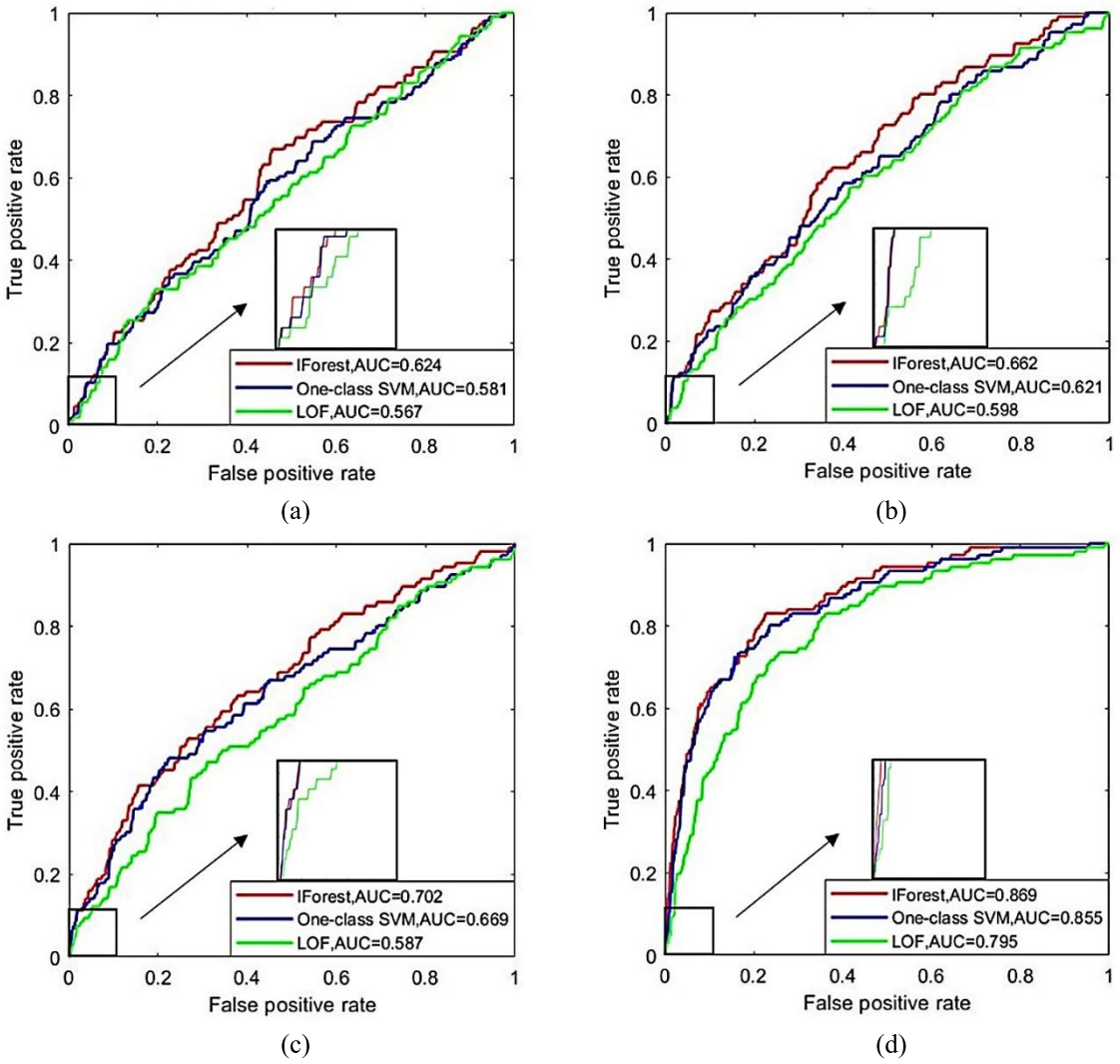

FIGURE 8. Comparison of three unsupervised learning algorithms. (a) ROC curves of three unsupervised learning algorithms ($\alpha = 0.9$, SNR $= -10$dB), (b) ROC curves of three unsupervised learning algorithms ($\alpha = 0.7$, SNR $= -10$dB), (c) ROC curves of three unsupervised learning algorithms ($\alpha = 0.9$, SNR $= -5$dB), (d) ROC curves of three unsupervised learning algorithms ($\alpha = 0.9$, SNR $= 0$dB).

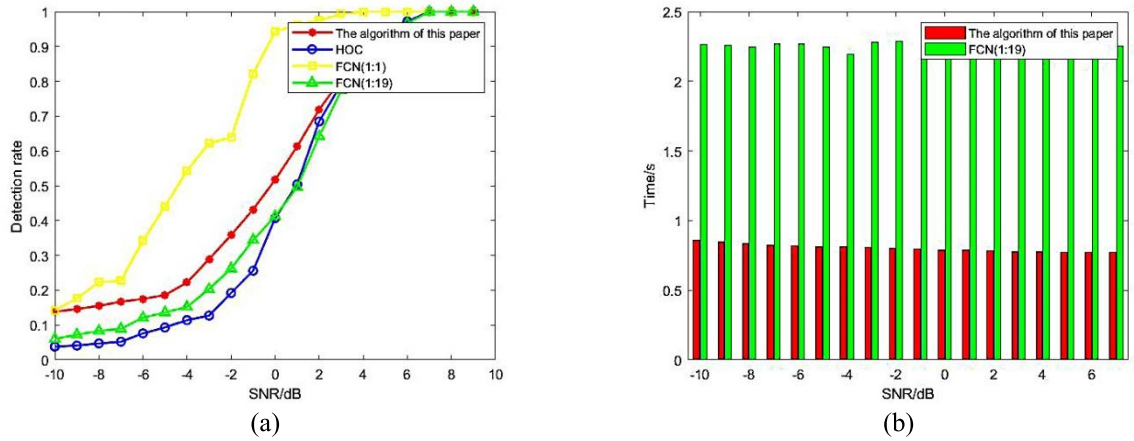

FIGURE 9. Performance comparison of different detection algorithms. (a) Detection probability of three methods in different SNRs, (b) Time-consuming comparison of the two algorithms.

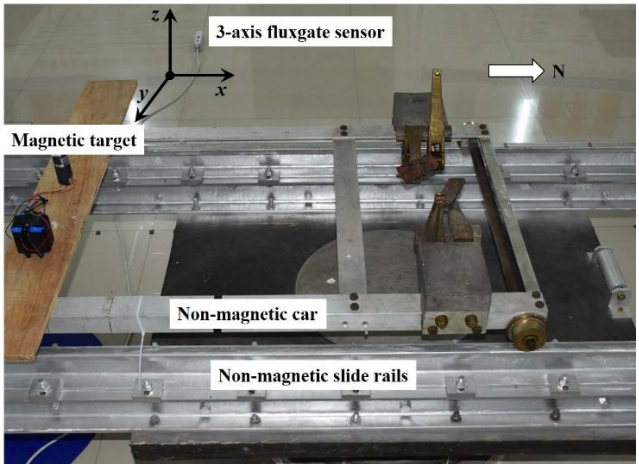

FIGURE 10. Experimental system setup.

The experimental time is 01:00-05:00 in the morning. Firstly, the pure geomagnetic environmental noise is monitored for a period of time to generate the negative sample data required for training. Then take the sensor position as the coordinate origin, the north direction is the positive direction of the x-axis, and the east direction is the positive direction of the y-axis to establish a rectangular coordinate system. Place the magnetic source on the non-magnetic trolley. The initial position of the magnetic source is (-10.5m, 1.1m, 0.75m). The trolley is driven by a stepper motor to move along the positive direction of the x-axis at a speed of 1m/s while the PC record magnetic field data. The experimental scene setup is shown in Fig.10.

Change the lateral distance between the sensor and magnetic source, take 10 measuring points, and generate positive sample data of different distances. Perform multiple sets of measurements at each measuring point, and change the direction of the magnetic source after each set of measurements, so that the positive samples cover the targets in various states as much as possible to avoid overfitting.

2) DATA PREPROCESSING

Fig.11(a) is a piece of original magnetic field data measured at a lateral distance of 1.5m from the magnetic source. It can be seen that the target signal is submerged in the geomagnetic background field and difficult to identify, so we need to preprocess the data. The slowly changing trend term and power frequency noise in the magnetic measurement signal are removed by band-pass filtering. In order to simplify the calculation, the data is Downsampling from 400Hz to 20Hz. The preprocessed signal waveform is shown in Fig.11(b). The sample data used for experimental verification refers to the preprocessed data.

As described in Section III-C, a period of time-series signal is divided into several samples by a sliding window. It is estimated that the duration of the magnetic source signal is about 5s, the length of the sliding window is set to 5.5s, and the moving step is 0.5s. Divide a piece of pure noise signal with a duration of about 505s after preprocessing into 1000 negative samples for training the IForest model, and randomly select 950 negative samples for training the FCN model. Measure the magnetic field data when the magnetic source is in motion. Repeat the measurement 5 times for each measuring point (the direction of the magnetic source is changed after each time is measured), and a total of $5 \times 10 = 50$ groups of mixed signals are generated. The ratio of positive and negative samples in the FCN training set is 50:950 = 1:19.

3) EXPERIMENTAL RESULTS AND ANALYSIS

Firstly, the IForest detection model is trained by the method in this paper; the FCN model is trained according to the paper [13] (the ratio of positive and negative samples in the training set is 1:19). Then place a magnetic source on the trolley, move the trolley, and measure 25 sets of magnetic field data at each measuring point. Finally input them into the detection model to calculate the output. Fig.12 shows the output of the IForest detection model when the signal shown in Fig.11 is input. It can be seen that this method can effectively suppress noise and accurately detect the target.

When the magnetic background noise is relatively stable, adjusting the lateral distance is equivalent to changing the SNR [34]. The method in this paper, FCN, and HOC were used to detect. Analyze their performance at different lateral distances. The results are shown in Fig.13.

It can be seen that the detection rate of the method in this paper is the highest, and the experimental results are consistent with the simulation results. Compared with HOC, the detection rate of the method is increased by about 4%-18%, which proves the superiority of fusion feature detection. Although the detection rate of FCN has been improved compared with that of HOC, it is seriously reduced when the positive and negative samples of the training set are unbalanced. When the horizontal distance is 1.7m, the detection rate of FCN is less than 40%, while the detection rate of the method in this paper is still above 50%. Compared with the FCN detection rate, the increase is about 4%-15%, which even exceeds the simulation test results. This is because the positive samples collected at different distances are not distinguished when training the FCN. Although the positive samples cover a variety of states of the target, the model does not sufficiently learn the various states. In contrast, the method in this paper can build a detection model with only a small number of negative samples and shows better detection performance under low SNR. The calculation shows that the method in this paper takes an average of 1.66×10^{-4}s to detect a sample, which is much smaller than the moving step of the sliding window, indicating that the method can meet the requirements of real-time detection.

The experimental environment set in this paper is ideal, and the interference of background magnetic anomalies on the results in the actual detection process is not considered.

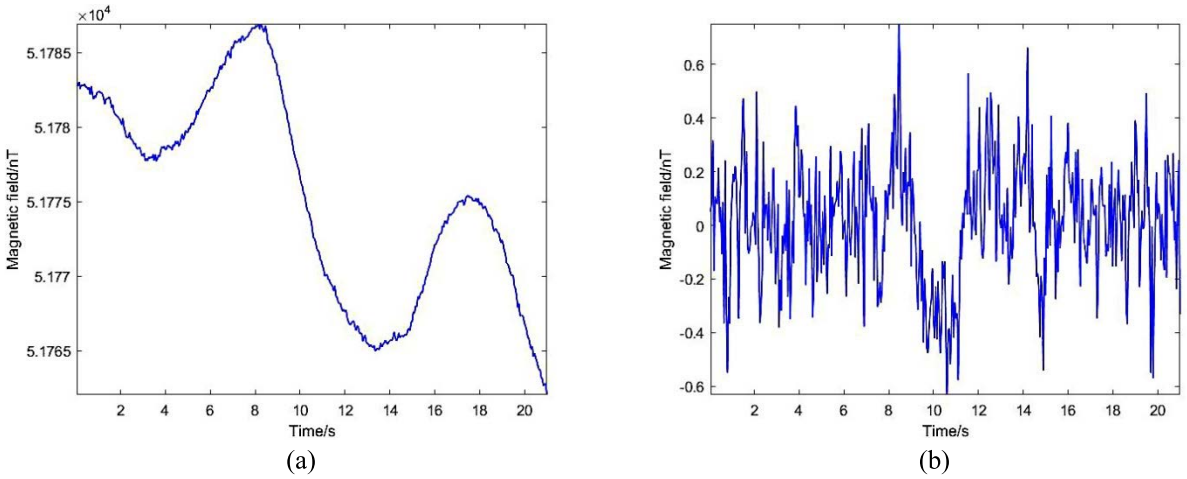

FIGURE 11. Data preprocessing. (a) Original signal, (b) Preprocessed signal.

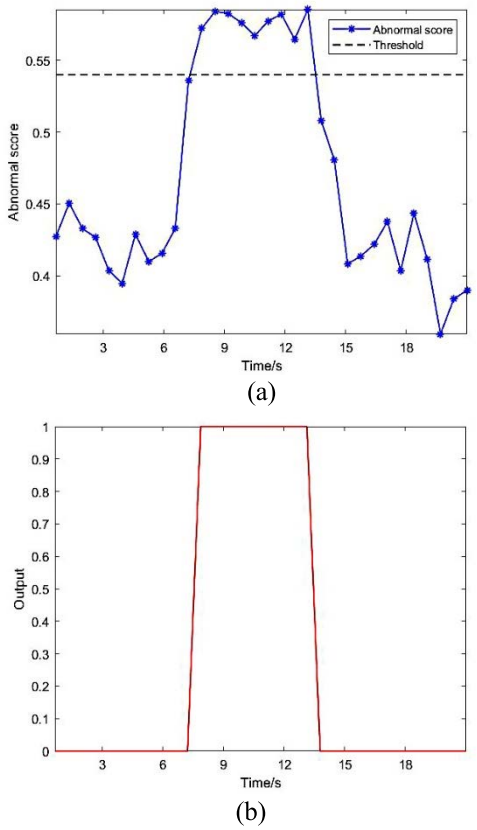

FIGURE 12. Output. (a) Abnormal score, (b) Detector output.

The trolley can be approximated to move in a straight line at a uniform speed on a non-magnetic guide rail, but in reality, the speed and trajectory of the flying carrier will fluctuate due to the influence of the airflow. Due to the existence of the non-orthogonal error of the three axes of the fluxgate sensor, the calculated total magnetic field value is inaccurate. These factors which are simplified in the experiment will affect the detection results.

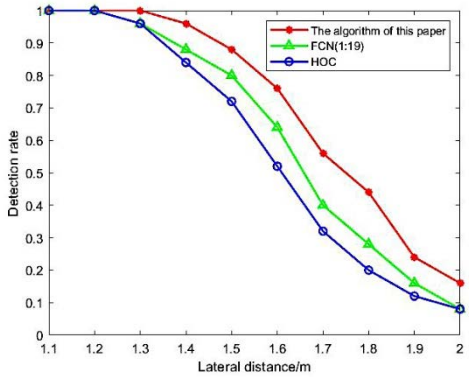

FIGURE 13. Detection rate of three methods under the experiment.

V. CONCLUSION

In this paper, a magnetic anomaly detection method based on feature fusion and isolation forest algorithm is proposed. The method extracts the statistical features, time-frequency features and fractal features of the magnetic anomaly signal and uses PCA to generate the fusion feature tensor, realizes the real-time target detection by the IForest algorithm. We studied and optimized the parameters of IForest model. The performance of the method is analyzed through simulation and experiment, and the conclusions are as follows:

1) Compared with unsupervised learning algorithms such as LOF and OS, the IForest used in this paper has an AUC improvement of 2%-11%, and this improvement is more obvious when the noise interference is strong.
2) The detection rate of proposed method is about 5%-18%higher than HOC, and the fusion feature is more suitable for magnetic target detection in the background of color noise.
3) The detection performance of FCN will decrease sharply when the positive and negative sample imbalance of

the training set. The method of this article can train an effective detection model with less negative samples. Compared with the FCN (1:19), the detection rate increases at 5%-12%.

4) This method does not need to model the target or background. The calculation is simple, and it is more suitable for real -time detection.

The PCA algorithm used in this method is a linear feature fusion method, so the effect is not obvious when dealing with nonlinear data. And the randomness of the IForest algorithm leads to unstable detection results. To deal with these problems, we will study non-linear feature fusion methods and more complicated unsupervised learning algorithms such as generative adversarial networks (GAN) for magnetic target detection to further improve the performance of weak magnetic detection. In addition, the experimental conditions designed in this paper are relatively ideal, but the actual geomagnetic environment noise is more complex, the shaking of the moving platform, the local geomagnetic anomaly caused by the geological structure and other factors will affect the detection results. The next step will be to design an external field aeromagnetic scale model test to further verify the effect of the method.

REFERENCES

[1] P. M. Dames, M. Schwager, D. Rus, and V. Kumar, "Active magnetic anomaly detection using multiple micro aerial vehicles," *IEEE Robot. Autom. Lett.*, vol. 1, no. 1, pp. 153–160, Jan. 2016.

[2] B. Jiangwei, W. Xuben, and G. Song, "Experimental aeromagnetic survey using a rotary-wing aircraft system: A case study in Heizhugou, Sichuan, China," *J. Appl. Geophys.*, vol. 184, Jan. 2021, Art. no. 104245.

[3] B. Ginzburg, L. Frumkis, and B. Z. Kaplan, "Processing of magnetic scalar gradiometer signals using orthonormalized functions," *Sens. Actuators A, Phys.*, vol. 102, nos. 1–2, pp. 67–75, Dec. 2002.

[4] C. Miao, Q. Dong, M. Hao, C. Wang, and J. Cao, "Magnetic anomaly detection based on fast convergence wavelet artificial neural network in the aeromagnetic field," *Measurement*, vol. 176, May 2021, Art. no. 109097.

[5] C. Wan, M. Pan, Q. Zhang, D. Chen, H. Pang, and X. Zhu, "Performance improvement of magnetic anomaly detector using Karhunen–Loeve expansion," *IET Sci., Meas. Technol.*, vol. 11, no. 5, pp. 600–606, Aug. 2017.

[6] Y. Tang, Z. Liu, M. Pan, Q. Zhang, C. Wan, F. Guan, F. Wu, and D. Chen, "Detection of magnetic anomaly signal based on information entropy of differential signal," *IEEE Geosci. Remote Sens. Lett.*, vol. 15, no. 4, pp. 512–516, Apr. 2018.

[7] Z. Wang, J. Qiu, D. Xie, J. Ou, and Q. Xu, "Weak magnetic anomaly signal detection based on the entropy of mixed differential signal," *AIP Adv.*, vol. 11, no. 1, Jan. 2021, Art. no. 015013.

[8] C. Wan, M. Pan, Q. Zhang, F. Wu, L. Pan, and X. Sun, "Magnetic anomaly detection based on stochastic resonance," *Sens. Actuators A, Phys.*, vol. 278, pp. 11–17, Aug. 2018.

[9] Y. Zhao, J. H. Zhang, J. H. Li, S. Liu, P. X. Miao, Y. C. Shi, and E. M. Zhao, "A brief review of magnetic anomaly detection," *Meas. Sci. Technol.*, vol. 32, no. 4, 2021, Art. no. 042002.

[10] J. Zheng, H. Fan, G. Yin, and Z. Li, "A method of using geomagnetic anomaly to recognize objects based on HOG and 2D-AVMD," *AIP Adv.*, vol. 9, no. 7, Jul. 2019, Art. no. 075015.

[11] K. Y. Zhang, M. K. Hu, C. P. Du, and M. Y. Xia, "Detection of magnetic dipole target signals by using convolution neural network," in *Proc. Cross Strait Quad-Regional Radio Sci. Wireless Technol. Conf. (CSQRWC)*, Jul. 2018, pp. 1–3.

[12] Y. Wang, Q. Han, G. Zhao, M. Li, D. Zhan, and Q. Li, "A deep neural network based method for magnetic anomaly detection," *IET Sci., Meas. Technol.*, vol. 16, no. 1, pp. 50–58, 2021.

[13] S. Liu, Z. Chen, M. Pan, Q. Zhang, Z. Liu, S. Wang, D. Chen, J. Hu, X. Pan, J. Hu, and P. Li, "Magnetic anomaly detection based on full connected neural network," *IEEE Access*, vol. 7, pp. 182198–182206, 2019.

[14] X. Xu, L. Huang, X. Liu, and G. Fang, "DeepMAD: Deep learning for magnetic anomaly detection and denoising," *IEEE Access*, vol. 8, pp. 121257–121266, 2020.

[15] Y. Zhenyu, "Research on underwater target identification technique based on MFP," Ph.D. dissertation, College Weapons Eng., Naval Univ. Eng., Wuhan, China, 2014.

[16] A. Sheinker, B. Ginzburg, N. Salomonski, P. A. Dickstein, L. Frumkis, and B. Z. Kaplan, "Magnetic anomaly detection using high-order crossing method," *IEEE Trans. Geosci. Remote Sens.*, vol. 50, no. 4, pp. 1095–1103, Apr. 2012.

[17] A. Sheinker, A. Shkalim, N. Salomonski, B. Ginzburg, L. Frumkis, and B.-Z. Kaplan, "Processing of a scalar magnetometer signal contaminated by $1/f^{\alpha}$ noise," *Sens. Actuators A, Phys.*, vol. 138, no. 1, pp. 105–111, Jul. 2007.

[18] W. X. Zhou, Y. Liu, and M. Q. Deng, "Research on intelligent fault diagnosis of rolling bearings under variable conditions based on CAE and CNN," *J. Chin. Soc. Power Eng.*, vol. 42, no. 1, p. 6, 2022.

[19] H. Wen, K. Longyun, and Y. Zongguang, "Planetary gearbox fault diagnosis based on variational mode decomposition with parameter optimization and multi-domain feature fusion," *Mach. Des. Res.*, vol. 37, no. 6, pp. 73–77, 2021.

[20] Q. F. Yu, Y. Q. Hu, and Y. Yang, "Arc fault detection based on wavelet feature and deep learning," *J. Electron. Meas. Instrum.*, vol. 34, no. 3, pp. 100–108, 2020.

[21] L. Chen, W. Zhu, P. Wu, C. Fei, and G. Fang, "Magnetic anomaly detection algorithm based on fractal features in geomagnetic background," *J. Electron. Inf. Technol.*, vol. 41, no. 2, pp. 332–340, 2019.

[22] Y. Yuan, Q. Wang, and G. Zhu, "Fast hyperspectral anomaly detection via high-order 2-D crossing filter," *IEEE Trans. Geosci. Remote Sens.*, vol. 53, no. 2, pp. 620–630, Feb. 2015.

[23] H. He, S. Zhao, W. Guo, Y. Wang, Z. Xing, and P. Wang, "Multi-fault recognition of gear based on wavelet image fusion and deep neural network," *AIP Adv.*, vol. 11, no. 12, Dec. 2021, Art. no. 125025.

[24] T. Yang, Z. C. Yang, and S. Y. Liang, "Time-frequency feature extraction and identification of stationary random dynamic load using deep neural network," *Acta Aeronautica et Astronautica Sinica*, to be published, doi: 10.7527/S1000-6893.2021.25952.

[25] X. Chun-Ling, C. Fei, S. Qing, X. Jian-Feng, and F. Xiao-Wei, "Sea-surface weak target detection based on multi-feature information fusion," *Syst. Eng. Electron.*, vol. 110, pp. 185–195, Jun. 2022.

[26] H. P. Wang, "Robust principal component analysis and its application on outlier detection," M.S. thesis, College Inf. Comput., Taiyuan Univ. Technol., Taiyuan, China, 2021.

[27] W. C. Guo, H. S. Zhao, and C. Li, "Fault feature enhancement method for rolling bearing fault diagnosis based on wavelet packet energy spectrum and principal component analysis," *Acta Armamentarii*, vol. 40, no. 11, pp. 2370–2377, 2019.

[28] F. T. Liu, K. M. Ting, and Z.-H. Zhou, "Isolation forest," in *Proc. 8th IEEE Int. Conf. Data Mining*, Dec. 2008, pp. 413–422.

[29] F. T. Liu, K. M. Ting, and Z. H. Zhou, "On detecting clustered anomalies using SCiForest," in *Machine Learning and Knowledge Discovery in Databases* (Lecture Notes in Computer Science), vol. 6322, J. L. Balcázar, F. Bonchi, A. Gionis, and M. Sebag, Eds. Berlin, Germany: Springer, 2010.

[30] C. B. Wan, "Investigations on the theory and method of magnetic anomaly detection," Ph.D. dissertation, College Artif. Intell., Nat. Univ. Defense Technol., Changsha, China, 2018.

[31] H. Sun, Z. W. Li, and X. Xiong, "Application and development of marine magnetic surveying technology," *Hydrographic Surveying Charting*, vol. 39, no. 6, pp. 5–8&20, 2019.

[32] Z. Y. Qian, Y.-H. Cao, L. Zhang, and H.-F. Qin, "Gear fault diagnosis based on dual-tree complex wavelet packet and SVM," *J. Command Control*, vol. 7, no. 4, pp. 415–423, 2021.

[33] G. Y. Zhao, "Research on interference mitigatiom and target detection of airborne magnetic anomaly detection," Ph.D. dissertation, School Comput. Sci. Technol., Harbin Inst. Technol., Harbin, China, 2019.

[34] L. Shuchang, "Investigations on magnetic anomaly detection based on neural network," Ph.D. dissertation, College Artif. Intell., Nat. Univ. Defense Technol., Changsha, China, 2019.

NING ZHANG was born in 1981. He received the Ph.D. degree from the Naval University of Engineering, Wuhan, China, in 2011. He is currently an Associate Professor with the Naval University of Engineering. His research interests include target's magnetic field study, aeromagnetic detection, and magnetic compensation.

YIFEI LIU was born in Weifang, Shandong, China, in 1997. He received the B.S. degree in mechanical engineering from the Wuhan University of Technology, in 2016. He is currently pursuing the M.S. degree with the Naval University of Engineering. His research interests include magnetic field study of target and magnetic source detection and location.

LEI XU was born in Zaoyang, Hubei, China, in 1993. He received the M.S. degree in performance test and fault diagnosis from Army Engineering University, Shijiazhuang, in 2018, and the Ph.D. degree from the Naval University of Engineering, in 2022. His research interests include magnetic field study of target and magnetic source detection and location.

PENGFEI LIN was born in Dongying, Shandong, China, in 1991. She received the B.S. degree in communication engineering from the China University of Petroleum (East China), in 2014, and the Ph.D. degree from the Naval University of Engineering, Wuhan, China, in 2021. She is currently a Lecturer with Dalian Naval Academy. Her research interests include target's magnetic field study and magnetic source detection and location.

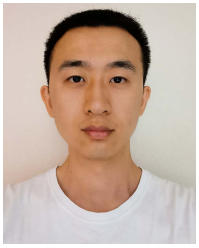

HEDA ZHAO was born in Heilongjiang, China, in 1993. He received the Ph.D. degree from the Naval University of Engineering, in 2021. His main research interests include target characteristics and information awareness technology.

MING CHANG was born in Kaifeng, Henan, China, in 1986. He received the B.S. and M.S. degrees from the Naval University of Engineering, where he is currently pursuing the Ph.D. degree. His research interests include target magnetic field characteristics, signal processing, and magnetic source tracking.